Available online at www.sciencedirect.com
SCIENCE DIRECT®
Journal of Solid State Chemistry 178 (2005) 3389–3395
JOURNAL OF SOLID STATE CHEMISTRY
www.elsevier.com/locate/jssc

A combined diffraction and dielectric properties investigation of $Ba_3MnNb_2O_9$ complex perovskites

Yun Liu[a], Ray L. Withers[a,*], A.P. Whichello[b], Lasse Norén[a], Valeska Ting[a], Frank Brink[a,c], John D. Fitz Gerald[d]

[a]*Research School of Chemistry, Australian National University, ACT 0200, Australia*
[b]*Centre for Advanced Telecommunications and Quantum Electronics Research, University of Canberra, ACT 2617, Australia*
[c]*Also at the ANU Electron Microscope Unit, Research School of Biological Sciences, Australian National University, ACT 0200, Australia*
[d]*Research School of Earth Sciences, Australian National University, Canberra, ACT 0200, Australia*

Received 18 May 2005; received in revised form 2 August 2005; accepted 28 August 2005
Available online 30 September 2005

Abstract

A combined synthesis, diffraction and dielectric properties investigation of the dependence (and effect) of Mn^{2+}/Nb^{5+} ordering in $Ba_3MnNb_2O_9$ (BMN) upon annealing atmosphere and processing conditions has been carried out. Annealing in different atmospheres was not found to significantly alter either nominal stoichiometry or structure type. The obtained structure type (disordered metrically cubic or ordered trigonal) as well as the measured electrical properties (in particular, the dielectric loss) were, however, found to be sensitive to the synthesis route. Samples obtained via solid-state reaction were found to be predominantly of 1:2 Mn^{2+}/Nb^{5+} ordered, $P\bar{3}m1$ trigonal structure type whereas samples obtained via an aqueous solution route were found to be of a Mn^{2+}/Nb^{5+} 'disordered', metrically cubic structure type. All solid-state synthesized samples showed reasonable dielectric properties. The microwave dielectric constant and dielectric quality factor, Q, at 8 GHz of an as-synthesized BMN sample were 38 and 100, respectively. By contrast, the dielectric loss of the metrically cubic, Mn^{2+}/Nb^{5+} 'disordered' samples obtained via an aqueous solution synthesis process were significantly worse.

Keywords: $Ba_3MnNb_2O_9$; Perovskite; Stacking faulting; Rietveld refinement; Dielectric property

1. Introduction

Dielectric materials with reasonably high dielectric constants, low dielectric losses and close to zero temperature coefficients of resonance have played a crucial role in recent progress in the field of microwave and satellite telecommunications. The $Ba_3M^{2+}(Nb,Ta)^{5+}O_9$ (M = Co, Ni, Mg, Zn and Mn) family of complex perovskites, in particular, have provided several compounds with extremely useful dielectric properties [1–5]. The additional ability to fine tune the properties of these compounds via appropriate doping and/or the formation of solid solutions with other member compounds is also of widespread interest and use. While much has been learnt about the correlation between the structures and dielectric properties of such materials, anomalies still remain to be understood.

$Ba_3MnNb_2O_9$ (BMN) is an intriguing member of this family of compounds. It has long been known that the addition of small amounts (~1–2%) of Mn to dielectric materials (including other members of the $Ba_3M^{2+}(Nb,Ta)^{5+}O_9$ family of complex perovskites) significantly improves both their sinterability as well as their microwave dielectric properties e.g. "... a small amount of Mn addition not only favourably affects the sinterability of the ceramics but also advantageously heightens the unloaded Q factor, to higher than 10^4 at 10 GHz ..." [6,7]. As a result, it has been in widespread use to modify the dielectric properties of $BaTiO_3$-based ceramics.

*Corresponding author. Fax: +61 2 6125 0750.
E-mail address: withers@rsc.anu.edu.au (R.L. Withers).

0022-4596/$ - see front matter © 2005 Elsevier Inc. All rights reserved.
doi:10.1016/j.jssc.2005.08.025

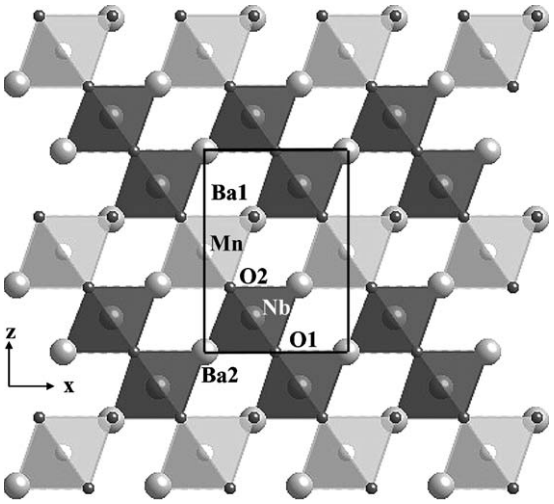

Fig. 1. $Ba_3MnNb_2O_9$ structure with the fully Mn^{2+}/Nb^{5+} ordered, $P\bar{3}m1$ trigonal structure of $Ba_3MnNb_2O_9$ in projection along the resultant $\boldsymbol{b}_h$ axis: MnO_6/NbO_6 octahedra (Mn: small light grey balls, Nb: medium sized dark grey balls), Ba atoms (largest grey balls) and O atoms (small dark grey balls).

The compound BMN itself is a quite complex and intriguing perovskite ceramic as regards structure/s, dielectric properties and the correlation between them. The earliest purely structural investigation reported a thermodynamically unstable 'disordered' cubic phase at lower temperature which underwent an irreversible phase transition to a 1:2 fully ordered, $P\bar{3}m1$ trigonal phase if synthesized and/or annealed at a sufficiently high temperature [8]. The first combined structural and dielectric properties investigation, that of Nomura [9], reported a Mn^{2+}/Nb^{5+} disordered, cubic perovskite ($a = 4.113$ Å) with a reasonable dielectric constant $\varepsilon = 39$, a rather low (relative to other members of the family) quality factor $Q = 100$ at 9.3 GHz and a reasonable temperature coefficient of the dielectric constant τ_ε of 27 ppm $^\circ C^{-1}$. Still later, Ranade and Salvi [10], in 1997, reported a significantly higher dielectric constant of 238 (at 400 Hz) and claimed that "… the XRD pattern … is dominated by 'disordered' cubic phase ($a = 4.104$ Å) reflections … except for … a couple of reflections indicating a tendency towards tetragonality …". They also claimed that the physical properties of BMN arose from "… local (Mn^{2+}/Nb^{5+}) compositional fluctuations …" and showed that BMN is "… a typical ferroelectric relaxor …" [10]. Most recently, Takahashi [11] calculated the phase stability of BMN using first-principles ab initio calculations. His conclusion was that BMN in equilibrium should be fully Mn^{2+}/Nb^{5+} ordered in the $P\bar{3}m1$ trigonal superstructure phase (see Fig. 1) commonly reported for $Ba_3M^{2+}B_2^{5+}O_9$ complex perovskites.

In view of these apparently conflicting reports as regards the structure/s and dielectric properties of BMN, it was decided to carefully reinvestigate Mn^{2+}/Nb^{5+} ordering in this compound, focussing on the effect of synthesis and processing conditions.

2. Experimental

Samples of nominal stoichiometry BMN were synthesized using both solid-state reaction (SSR) as well as via an aqueous solution (AS) route. Barium carbonate ($BaCO_3$, 3 N, Noah), manganese dioxide (MnO_2, 80%, AJAX) and niobium (V) oxide (Nb_2O_5, >3 N, Alfa) were used as starting materials for the SSR route. Powders of the desired stoichiometry were thoroughly mixed in a mortar and then heated at 850 °C for an initial period of 20 h. The resultant powder was then re-mixed, pressed into a pellet and sintered at 1350 °C for a period of 5 days with intermediate grinding and repelleting.

Barium acetate ($Ba(CH_3COO)_2$, 99%, Pto Analytical), manganese (II) acetate tetrahydrate ($(C_2H_3O_2)_2Mn \cdot 4H_2O$, 99 + %, Aldrich), and niobium (V) chloride ($NbCl_5$, 99%, Aldrich) were chosen as starting materials for the AS route. A uniform emulsion was initially obtained at room temperature by mixing these starting ingredients together. This solution was then dried at 200 °C followed by heat-treatment at 600 °C overnight. The resultant powders were then re-ground and heated at 850 °C for a day prior to a final annealing at 1300 °C for a further 3 days. Subsequently, the resultant pellets were heat-treated around 1000 °C in different atmospheres (N_2, O_2 and Ar).

Electron probe microanalysis (EPMA) was used to determine composition at 15 kV and 1 nA using a JEOL 6400 scanning electron microscope (SEM) equipped with an Oxford Instruments light element EDS detector and Link ISIS SEMquant software. Samples were prepared by mounting the prepared powders in resin, polishing to a <1 μm finish followed by the application of a thin carbon coat. Rhodonite ($MnSiO_3$), NbO_2F and Barite ($BaSO_4$) were chosen as internal calibration standards. Five spot analyses were collected from each sample.

The resultant samples were then carefully investigated by powder X-ray diffraction using a Guinier-Hägg camera with a $CuK_{\alpha 1}$ radiation source. Si (NBS#640c, $a = 5.431195(9)$ Å at 22.5 °C) was used as an internal standard in order to accurately determine unit cell parameters through the 'Unitcell' software package [12].

The electron diffraction patterns (EDPs) were recorded in a Philips EM 430 Transmission Electron Microscope (TEM) on crushed grains of the samples dispersed onto holey carbon-coated copper grids. The HREM lattice images were obtained on the same samples using a Philips CM 300 TEM.

The neutron powder diffraction pattern of the Mn^{2+}/Nb^{5+} ordered BMN sample was collected using neutrons of wavelength 1.883 Å over the 2θ range $10^\circ < 2\theta < 148^\circ$ employing a step size of 0.05°. An aluminium-capped vanadium cylinder was used as the sample holder on the High-Resolution Powder Diffractometer at the High Flux Australian Reactor (HIFAR) operated by the Australian Nuclear Science and Technology Organization (ANSTO). The structure refinement was undertaken using the Rietveld program Rietica [13]. The background was fitted

using a polynomial with six refinable parameters. The zero point was then refined. The variation in peak shape was described with a pseudo-Voigt function with three half-width parameters and a further parameter to describe a fixed shape of any type between Gaussian and Lorentzian forms. The other parameters varied were the atomic coordinates, the atomic displacement parameters, the occupancies and the unit cell parameters.

Both sides of the resultant pellets were also polished and then brushed with silver conductive paste followed by heat treatment at 550 °C for 30 min in order to ensure good electrical contact. The dielectric properties (dielectric constant and loss) were then measured using a high-precision LCR meter (Agilent 4284A) while the resistivity was measured with a multimeter (HP3478A) using the four-probe method. The dielectric properties at microwave frequencies were obtained using a HP8510A network analyzer via a resonant model.

3. Results and discussion

3.1. Compositional analysis

From EPMA, annealing in different atmospheres made very little difference to the stoichiometry of the samples synthesized via the SSR route. All average compositions were $Ba_{1.00(1)}Mn_{0.34(1)}Nb_{0.66(1)}O_3$, very close to the nominal BMN stoichiometry. The resultant composition of the samples obtained via the AS route was $Ba_{0.97(2)}Mn_{0.33(2)}Nb_{0.67(1)}O_{2.97}$ for the as-made sample and $Ba_{0.98(1)}Mn_{0.35(1)}Nb_{0.65(1)}O_{2.96}$ for the sample heat-treated at 950 °C in an oxygen atmosphere, again very close to the nominal BMN stoichiometry.

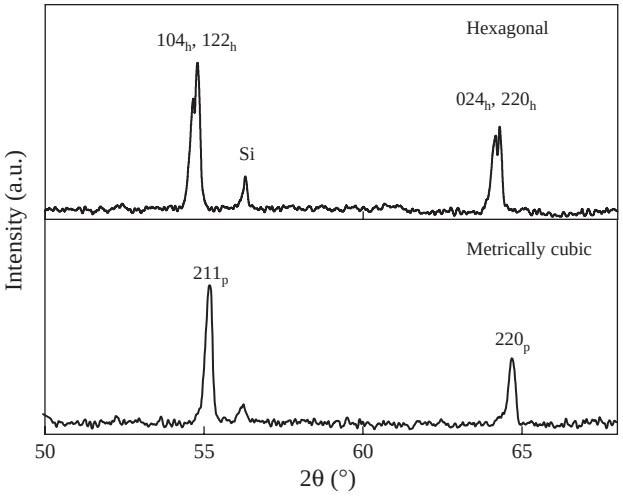

Fig. 2. Typical scanned traces of a relatively high angle portion of the XRD patterns of BMN samples obtained via the SSR (hexagonal) and AS (metrically cubic) routes.

3.2. XRD

The BMN samples obtained via the SSR and AS routes were both single phase. Their metric symmetries, however, differ. Fig. 2 shows typical scanned traces of a relatively high angle portion of the XRD patterns of both sample types. The AS samples are metrically cubic ($a = 4.1098(4)$ Å). The clear splitting of the parent perovskite lines (the top trace in Fig. 2) in the case of the SSR samples, however, requires a lowering of the metric symmetry to hexagonal. The Guinier films of the as-made SSR samples are consistent with a space group symmetry of $P\bar{3}m1$ ($a = b = 5.8125(5)$ Å and $c = 7.1438(9)$ Å), as might be expected for a Mn^{2+}/Nb^{5+} ordered perovskite of composition BMN (see Fig. 1). These lattice parameters are only very slightly changed after heat-treatment in the various different atmospheres (Ar: $a = 5.8115(6)$ Å and $c = 7.1364(9)$ Å; O_2: $a = 5.8093(8)$ Å and $c = 7.1347(14)$ Å; N_2: $a = 5.812(9)$ Å and $c = 7.1293(14)$ Å). The differing metric symmetries obtained via the SSR and AS routes presumably result from the different extent of mixing of the raw materials on the fine scale (the AS route would be expected to provide a more homogeneous initial mixing at the molecular level). As a result, the reaction energy, reaction order and crystallization energy might be different. In addition, BMN itself also has a tendency to disordered Mn/Nb ordering as discussed below. Note that the 1:2 ordered BMN phase is quite stable so that increasing the annealing time at 1350 °C did not transform it into the disordered cubic phase.

3.3. Electron microscopy

Fig. 3 shows typical $\langle 110 \rangle_p$ (subscript p for underlying perovskite parent structure) EDPs of the (a) Mn^{2+}/Nb^{5+} ordered, $P\bar{3}m1$ ($\mathbf{a}_h = \mathbf{b}_p - \mathbf{c}_p$, $\mathbf{b}_h = \mathbf{c}_p - \mathbf{a}_p$, $\mathbf{c}_h = \mathbf{a}_p + \mathbf{b}_p + \mathbf{c}_p$; $\mathbf{a}_h^* = \frac{1}{3}[\bar{1}2\bar{1}]_p^*$, $\mathbf{b}_h^* = \frac{1}{3}[\bar{2}11]_p^*$, $\mathbf{c}_h^* = \frac{1}{3}[111]_p^*$) metrically hexagonal phase obtained in the case of the SSR samples and (c) the nominally Mn^{2+}/Nb^{5+} disordered, metrically cubic phase obtained in the case of the AS route samples. Fig. 3b shows the composite EDP that results when more than one twin variant of the hexagonal phase is simultaneously illuminated. Note the similarity between this EDP (Fig. 3b) and the EDP characteristic of the nominally Mn^{2+}/Nb^{5+} disordered, metrically cubic phase shown in Fig. 3c. This suggests that the apparent 'disorder' of the metrically cubic phase is illusory and may in fact result from fine-scale orientational twinning and stacking faulting of the fully ordered trigonal phase on the four $\{111\}_p$ planes.

Direct evidence for such microstructural faulting is given in Fig. 4. The $\langle 01\bar{1} \rangle_p$ HREM lattice image of Fig. 4a, for example, shows an orientational twin boundary in the 1:2 ordered phase (the corresponding FFT composite EDP is shown inset—cf. with Fig. 3b). In the bottom half of Fig. 4a, the $(001)_h^1$ superlattice planes of the first orientational variant are clearly apparent (sight along the white arrow) while those of the second orientational variant are

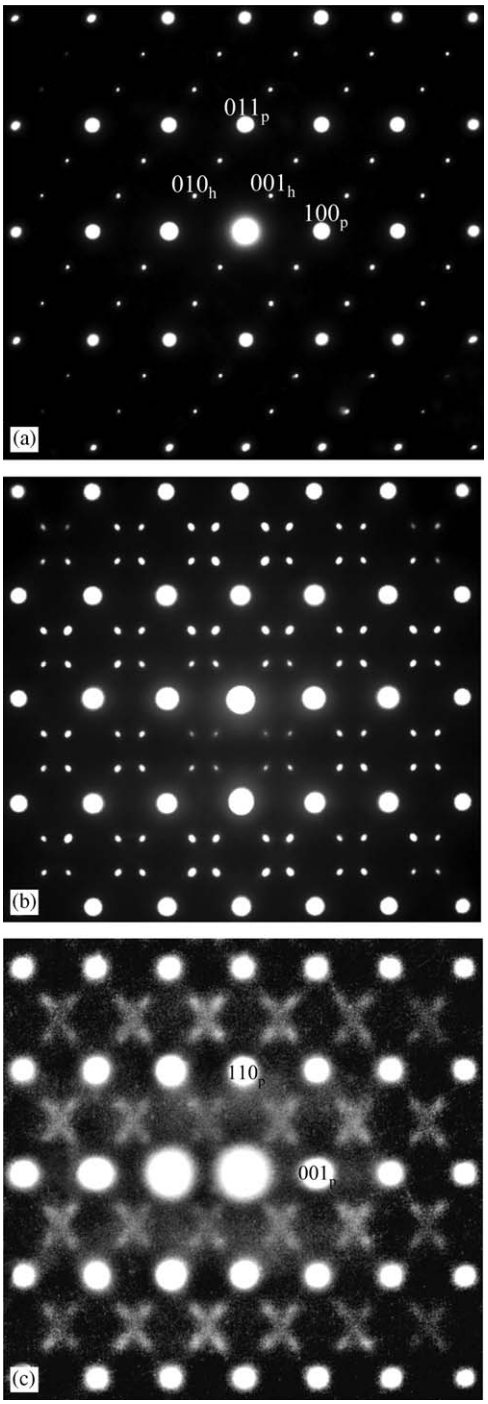

Fig. 3. Typical $\langle 110 \rangle_p$ EDPs of the (a) Mn^{2+}/Nb^{5+} ordered, $P\bar{3}m1$ metrically hexagonal phase obtained in the case of the SSR samples and (c) the nominally Mn^{2+}/Nb^{5+} disordered, metrically cubic phase obtained in the case of the AS route samples. Fig. 3b shows the composite EDP that results when more than one twin variant of the hexagonal phase is simultaneously illuminated. Indexation with the subscript p in (a) is with respect to the underlying parent perovskite average structure while that with the subscript h is with respect to the resultant $P\bar{3}m1$ metrically hexagonal structure.

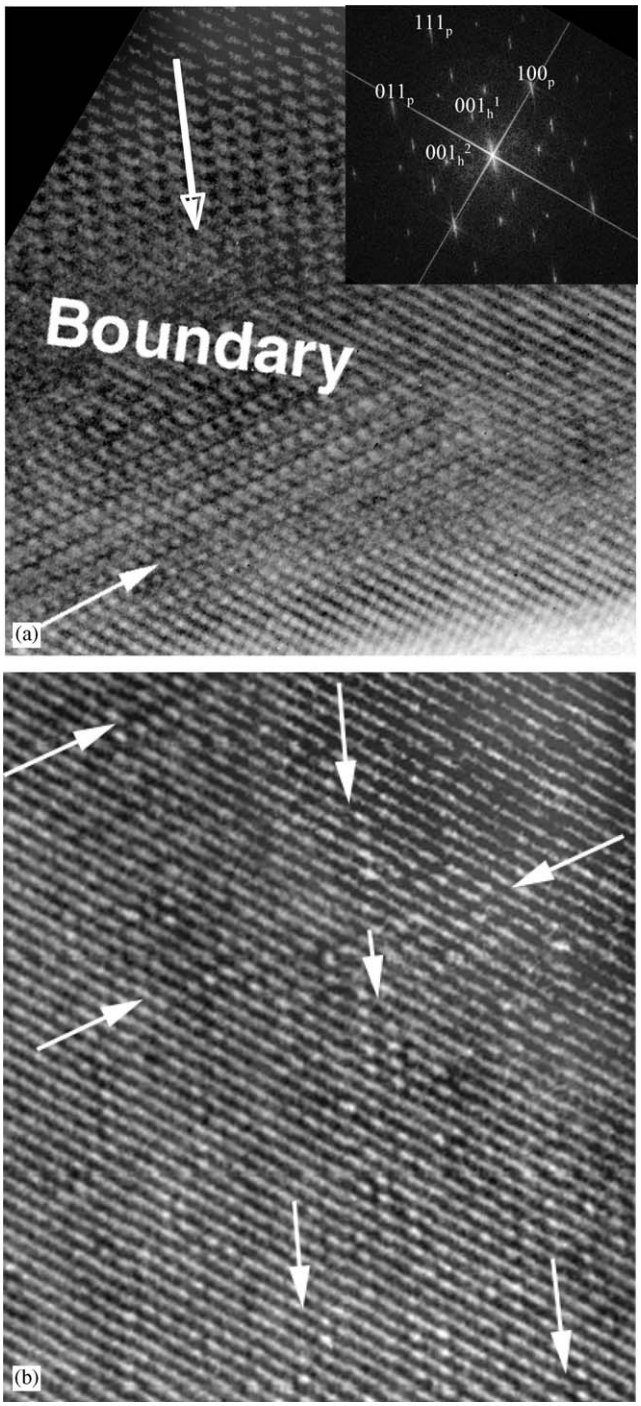

Fig. 4. (a) An $\langle 01\bar{1} \rangle_p$ HREM lattice image of an orientational twin boundary occurring within the the 1:2 ordered BMN phase (the corresponding FFT composite EDP is shown inset). The $(001)_h^1$ superlattice planes of the first orientational twin variant are apparent in the bottom half of (a) (by sighting along the white arrow) while those of the second orientational variant are apparent in the top half of the figure (again by sighting along the white arrow). Vestiges of the same superlattice planes are apparent in the equivalent $\langle 01\bar{1} \rangle_p$ HREM lattice image of the disordered 'cubic' phase shown *q* in Fig. 4b (again sight along the white arrows).

also clearly apparent in the top half of the figure (again sight along the white arrow). Vestiges of the same superlattice planes are apparent in the equivalent $\langle 01\bar{1} \rangle_p$ HREM lattice image of the disordered 'cubic' phase shown in Fig. 4b (again sight along the white arrows). In this case, however, the supercell/s have an extremely limited

correlation length or 'domain size' along the $\langle 001\rangle_h^*$ directions (and hence are streaked out along this direction) and a rather longer correlation length perpendicular to this direction (corresponding to the strings of white dots apparent from sighting along the arrows in Fig. 4b) giving rise to the diffuse crosses of Fig. 3c.

Similar short-range nano-domain ordering was first reported for $BaZrO_3$-doped $Ba_3ZnTa_2O_9$ and $Ba_3NiTa_2O_9$ and a direct connection established between the degree and length scale of this cation disorder and changes in the dielectric loss properties (see e.g. [14,15]). Note that the diffuse crosses centred on the $\mathbf{G}\pm\frac{1}{2}\langle 111\rangle_p^*$ regions of reciprocal space and extending from $\mathbf{G}\pm\frac{1}{3}\langle 111\rangle_p^*$ to $\mathbf{G}\pm\frac{2}{3}\langle 111\rangle_p^*$ in Fig. 3c are quite weak and hard to record. They are nonetheless always present and quite characteristic of this 'phase'.

3.4. Neutron diffraction

In view of the fact that a refined structure for the Mn^{2+}/Nb^{5+} ordered, $P\bar{3}m1$ ($\mathbf{a}_h=\mathbf{b}_p-\mathbf{c}_p$, $\mathbf{b}_h=\mathbf{c}_p-\mathbf{a}_p$, $\mathbf{c}_h=\mathbf{a}_p+\mathbf{b}_p+\mathbf{c}_p$; $\mathbf{a}_h^*=\frac{1}{3}[\bar{1}2\bar{1}]_p^*$, $\mathbf{b}_h^*=\frac{1}{3}[\bar{2}11]_p^*$, $\mathbf{c}_h^*=\frac{1}{3}[111]_p^*$) metrically hexagonal phase has yet to be reported, neutron diffraction data of the as-made BMN sample were collected and refined (see Fig. 5). A fully *B*-site ordered model of trigonal $P\bar{3}m1$ space group symmetry (with six independent atom sites and four refineable fractional co-ordinate parameters—see Table 1) was initially assumed. Refinement proceeded smoothly and convergence was rapidly achieved. The resultant profile fit is essentially identical to that shown in Fig. 5. The final refinement statistics for this model using Rietica were: $R_p=7.02$, $R_{wp}=8.72$, GOF = 1.34 and $R_{Bragg}=1.53$ and clearly constitute a quite acceptable refinement. The refined fractional co-ordinates along with the calculated bond valence sums (or apparent valences, AVs [16]) are given in Table 1. Note that the refined isotropic atomic displacement parameter (or B factor) of the Mn ions for this fully ordered refinement model (see the first line of Table 1) is significantly larger than for the other ions.

This suggested to us that it might well be due to stacking fault disorder of the Mn^{2+}/Nb^{5+} ions, in the same manner as discussed previously for $Ba_3CoNb_2O_9$ [17]. The particular translational stacking faulting envisaged is characterized by displacive shifts of the whole $P\bar{3}m1$, trigonal superstructure across stacking faults within individual orientational domains of $\pm\mathbf{R}$ (where $\mathbf{R}\sim\mathbf{c}_p=\frac{1}{3}[-\mathbf{a}_h+\mathbf{b}_h+\mathbf{c}_h]$). The effect of such translational stacking faulting is, of course, to appear to put some Mn^{2+} on the Nb^{5+} sites and vice-versa. The refinement process used for modelling such stacking faulting is the same as that described in [17]. Refinement again proceeded smoothly and converged rapidly. The final refinement statistics obtained using this model were: $R_p=6.99$, $R_{wp}=8.68$, GOF = 1.33 and $R_{Bragg}=1.32$. The final resultant profile fit is shown in Fig. 5. All the refinement statistics parameters decrease and in particular, the R_{Bragg} is significantly reduced, indicating a better model. The final refined structural parameters are listed in the second lines of Table 1 while an $[010]_h$ projection of the resultant structure is shown in Fig. 1. Note that the refined isotropic atomic displacement parameter of the Mn ions is thereby significantly decreased.

The initial apparent overbonding and underbonding of the Mn and Nb ions is also marginally improved. The refinement suggests that there are 1.85% of each of the alternative stacking fault variants present. The positioning of these variants relative to the dominant variant are given by the displacive shift vectors $\pm\mathbf{R}=\pm\left[\frac{1}{3},\frac{1}{3},\frac{1}{3}+\delta\right]_h$, where δ refined to 0.01(1). The shift is quite subtle and does not significantly affect the average structure. It does, however, give a slightly improved structure from the local crystal chemical point of view. It also suggests the type of disorder that could well be responsible for BMN appearing to have cubic metric symmetry (see below).

Table 1
Refined structural parameters and the corresponding bond valence sum (AV) values obtained for a fully *B*-site ordered refinement (first lines) and a stacking faulted refinement (second lines) of BMN

Atom	*x*	*y*	*z*	*B*	*n*	AV
Mn	0.0000	0.0000	0.5000	1.20 (17)	1.00	2.209
	0.0000	0.0000	0.5000	0.50 (21)	0.963 (8)	2.162
Nb	0.3333	0.6667	0.1740 (4)	0.48 (5)	1.00	4.737
	0.3333	0.6667	0.1739 (5)	0.35 (5)	0.963 (8)	4.796
Ba1	0.3333	0.6667	0.6659 (4)	0.54 (5)	1.00	2.195
	0.3333	0.6667	0.6662 (7)	0.60 (5)	0.963 (8)	2.191
Ba2	0.0000	0.0000	0.0000	0.54 (5)	1.00	2.339
	0.0000	0.0000	0.0000	0.60 (5)	0.963 (8)	2.345
O1	0.5000	0.0000	0.0000	0.75 (3)	1.00	1.984
	0.5000	0.0000	0.0000	0.79 (3)	0.963 (8)	1.987
O2	0.1732 (2)	0.3464 (4)	0.3216 (4)	0.75 (3)	1.00	2.076
	0.1737(3)	0.3474 (5)	0.3207 (5)	0.79 (3)	0.963 (8)	2.087

Fully *B*-site ordered model: $a=b=5.81249(7)$ Å and $c=7.14368(12)$ Å.
Stacking faulted model: $a=b=5.81252(7)$ Å and $c=7.14373(12)$ Å.

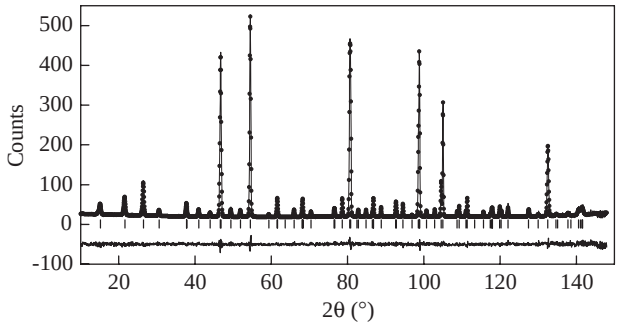

Fig. 5. The final resultant profile fit for the stacking faulted, Mn^{2+}/Nb^{5+} ordered, $P\bar{3}m1$ structure of BMN.

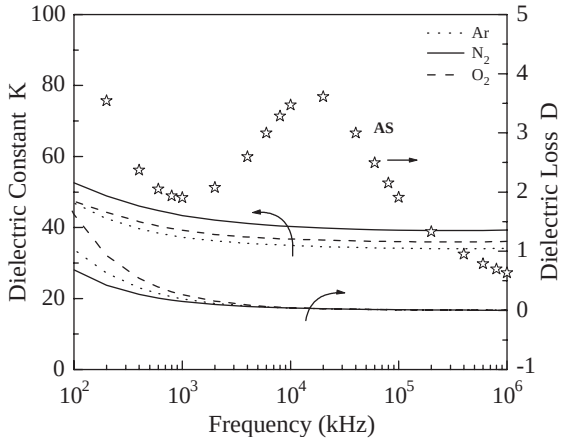

Fig. 6. Shows the measured room temperature dielectric constants and dielectric losses of the SSR synthesized BMN samples annealed under Ar, N_2 and O_2 as a function of frequency from 100 Hz to 1 MHz. The dielectric loss of the AS-synthesized sample is also shown.

3.5. Electrical properties

The room temperature dielectric constants and dielectric losses of various BMN samples were also measured as a function of frequency from 100 Hz to 1 MHz as shown in Fig. 6. The bulk densities of the fired BMN pellets were determined by the liquid displacement method to be 5.99 g/cm^3, corresponding to a theoretical density of 95%. The samples synthesized via the SSR route always showed rather low dielectric losses, essentially independent of frequency above ~1 kHz and independent of the annealing atmosphere used. In the lower-frequency range (<1 kHz), the dielectric loss of the sample heat treated in O_2 is slightly higher than the samples heat treated in Ar and N_2. By contrast, the dielectric losses of the samples prepared by the AS route were always significantly higher suggesting that apparent Mn^{2+}/Nb^{5+} disordering caused by twinning and stacking faulting has a significant deleterious effect upon the dielectric properties of BMN.

The measured dielectric constants of the SSR samples ranged from ~35 to 55 (over the frequency range measured), in far better agreement with the value of 39 (at 9.3 GHz) reported by Nomura [9] than with the value of 238 (at 400 Hz) reported by Ranade and Salvi [10]. This result led us to investigate the dielectric properties of the SSR samples at microwave frequencies. The resonant frequency of the as-made SSR sample was found to be 8 GHz. At this microwave frequency, the dielectric constant was evaluated to be around 38 and the Q value around 100, in excellent agreement with the reported results of Nomura [9].

As stated above, the samples from the AS route always showed a quite high dielectric loss, particularly at low frequency. Indeed, the low-frequency loss was high enough that the AS samples are room temperature semiconductors with a resistivity around $3 \times 10^5\,\Omega\cdot$cm. The peak in the dielectric loss around around 10^4 kHz suggests some sort of low-frequency structural relaxation perhaps associated with the structural disorder suggested by Fig. 3c.

4. Interpretation of the observed structured diffuse scattering

Given the effect that Mn^{2+}/Nb^{5+} disordering has upon the measured dielectric loss properties, it is of some practical, as well as inherent, interest to understand the nature of this disordering. The observed streaking along the $\langle 111\rangle^*_p$ directions apparent in $\langle 110\rangle_p$ zone axis EDPs of the disordered, metrically cubic phase (see Fig. 3c) requires that the disorder arises from $\{111\}_p$ planar faulting, presumably $\{111\}_p$ planar stacking faulting associated with the pattern of Mn^{2+}/Nb^{5+} ordering.

Consider the fully 1:2 Mn^{2+}/Nb^{5+} ordered, $P\bar{3}m1$ trigonal structure shown in Fig. 1. From a modulation wave point of view, the Mn^{2+}/Nb^{5+} ordering along the $\mathbf{c}_h = [111]_p$ direction of this structure type can be described by the square wave type compositional Atomic Modulation Function (AMF) shown in Fig. 7. Such a compositional AMF describes the compositional deviation, δf_B, of the B site metal ions away from the average B site occupancy of $\bar{f}_B = (\frac{1}{3}\mathrm{Mn} + \frac{2}{3}\mathrm{Nb})$ as a function of $\bar{x}_4 = \mathbf{q}(\mathbf{r}_\mu + \mathbf{t})$, where $(\mathbf{r}_\mu + \mathbf{t})$ represents the positioning of the different B site layers perpendicular to $[111]_p$ and the primary modulation wave-vector $\mathbf{q} = \frac{1}{3}[111]^*_p$ for the fully Mn^{2+}/Nb^{5+} ordered, $P\bar{3}m1$ trigonal structure [18,19]. (For those unfamiliar with this modulated structure AMF approach, a more detailed recent application of this approach to disordered materials is given in [20].)

Clearly such a compositional AMF implies the …–Mn–Nb–Nb–Mn–Nb–Nb–… ordering observed experimentally (cf. with Fig. 1) for $\mathbf{q} = \frac{1}{3}[111]^*_p$. In the case of the Mn^{2+}/Nb^{5+} disordered, metrically cubic structure, the diffuse streaking along $\langle 111\rangle^*_p$ observed experimentally ranges from $\mathbf{q} = \frac{1}{3}[111]^*_p$ all the way to $\mathbf{q} = \frac{1}{2}[111]^*_p$ (see Fig. 3c) and implies the co-existence of …–Mn–Nb–Nb—Mn–Nb–Nb–… ordering as would be expected for $\mathbf{q} = \frac{1}{3}[111]^*_p$ with the …–Mn–Nb–Mn–Nb–… and …Nb–Nb–Nb–Nb–… ordering patterns that could arise for $\mathbf{q} = \frac{1}{2}[111]^*_p$ (dependent upon the initial starting point or global phase used). Note that the magnitude range of the

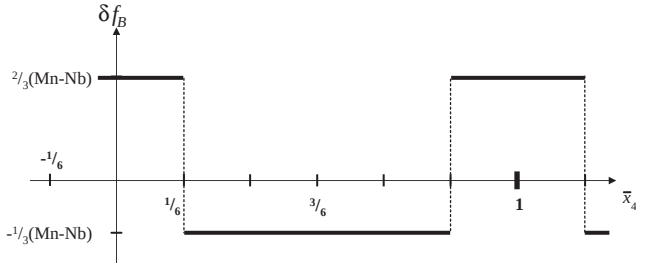

Fig. 7. Compositional AMF describing the compositional deviation, δf_B, of the B site metal ions away from the average B site occupancy of $\bar{f}_B = (\frac{1}{3}\mathrm{Mn} + \frac{2}{3}\mathrm{Nb})$ as a function of $\bar{x}_4 = \mathbf{q}(\mathbf{r}_\mu + \mathbf{t})$.

observed modulation wave-vectors i.e. $\frac{1}{3}<q<\frac{1}{2}$ rules out the possibility of neighbouring Mn occupied (111) layers. This would require modulation wave-vector magnitudes $q<\frac{1}{3}$ e.g. suppose $\bar{x}_4$ was very slightly greater than $-\frac{1}{6}$ in Fig. 7 corresponding to a Mn layer, then the following layer could only be a Mn layer if $(q-\frac{1}{6})$ were less than $\frac{1}{6}$ i.e. if $q<\frac{1}{3}$. Experimentally, however, this is not the case (see Fig. 3b).

Modulation wave-vector magnitudes intermediate between $q=\frac{1}{3}$ and $q=\frac{1}{2}$ such as, for example, $q=\frac{5}{12}$, not surprisingly, generate mixtures of the above local Mn/Nb ordering distributions. The observed diffuse streaking in Fig. 3c then implies a mixture of …–Mn–Nb–Nb–Mn–Nb–Nb–…, …–Mn–Nb–Mn–Nb–… and … Nb–Nb–Nb–Nb–… ordering within a single orientational domain. It may be that the implied presence of Mn/Nb/Mn/Nb ordering may be a result of local oxidation of Mn^{2+} to Mn^{3+} although the EPMA results suggest than any such oxidation must be limited.

The presence of diffuse crosses in Fig. 3c requires that this stacking faulting along a particular $[111]_p$ direction is also accompanied, on a fairly regular scale, by rotational twinning whereby the unique local $[111]_p$ axis along which the Mn^{2+} and Nb^{5+} ions are ordering changes between the four distinct possible such $\langle 111\rangle_p$ directions. Direct evidence for such fine-scale orientational twinning is apparent in Fig. 4b.

The deleterious effects of such fine-scale microstructural faulting upon dielectric properties, in particular upon microwave dielectric loss properties, must then be associated with the local structural relaxation at the fault planes. It would be of some interest to understand this phenomenon in more detail. This, however, is beyond the scope of the current contribution.

5. Conclusion

Dependent upon the synthesis route and processing conditions, it is clear that BMN can be found either in the form of a 1:2 Mn^{2+}/Nb^{5+} ordered, $P\bar{3}m1$ trigonal structure type or in the form of a Mn^{2+}/Nb^{5+} 'disordered', metrically cubic structure type. It is also clear that the dielectric properties, in particular the dielectric loss properties, are strongly dependent upon the extent of Mn^{2+}/Nb^{5+} ordering. Structured diffuse scattering observed in the case of the Mn^{2+}/Nb^{5+} disordered, metrically cubic structure suggests that the apparent disorder arises from fine-scale $\{111\}_p$ stacking faulting and rotational twinning.

Acknowledgments

The authors would like to thank Dr. Margaret Elcombe of the Australian Nuclear Science and Technology Organization for her help with the collection of the neutron data, and would also like to thank the Australian Institute of Nuclear Science and Technology for their financial support (AINSE Award 2005, Project no. AINGRA 05176). YL and RLW acknowledge financial support from the Australian Research Council (ARC) in the form of an ARC Discovery Grant.

References

[1] Y.S. Cho, K.H. Yoon, B.D. Lee, H.R. Lee, E.S. Kim, Ceram. Intern. 30 (2004) 2223–2227.
[2] L. Abdul Khalam, H. Sreemoolanathan, R. Ratheesh, P. Mohanan, M.T. Sebastian, Mater. Sci. Eng. 107 (2004) 264–270.
[3] S.G. Lee, C.I. Kim, J.P. Kim, S.H. Lee, Mater. Lett. 58 (2004) 110–114.
[4] S.K. Manik, S.K. Pradhan, Mater. Chem. Phys. 86 (2004) 284–292.
[5] I.M. Reaney, P.L. Wise, I. Qazi, C.A. Miller, T.J. Price, D.S. Cannell, D.M. Iddles, M.J. Rosseinsky, S.M. Moussa, M. Bieringer, J. Eur. Ceram. Soc. 23 (2003) 3021–3034.
[6] N. Shoichiro, Ferroelectrics 49 (1–4) (1983) 61–70.
[7] T. Nishimura, T. Suzuki, Y. Watanabe, Reduction-resistant dielectric ceramic composition and laminated ceramic capacitor. Japanese patent: JP 06084408, 1994.
[8] U. Treiber, S. Kemmler-Sack, J. Solid State Chem. 43 (1982) 51–62.
[9] S. Nomura, Ferroelectrics 49 (1983) 61–70.
[10] A.J. Ranade, S.V. Salvi, Ferroelectrics 197 (1-4) (1997) 815–820.
[11] T. Takahashi, Jpn. J. Appl. Phys. 39 (2000) 5637–5641.
[12] B. Noläng, Inst. Materialkemi, Ängströmlaboratoriet, Box 538, SE-751 21, Uppsala, Sweden.
[13] B.A. Hunter, Rietica—A Visual Rietveld Program, Commission on Powder Diffraction Newsletter 20 (1998) 21.
[14] P.K. Davies, J. Tong, T. Negas, J. Am. Ceram. Soc. 80 (1997) 1727–1740.
[15] L. Chai, P.K. Davies, J. Am. Ceram. Soc. 80 (1997) 3193–3198.
[16] N.E. Brese, M. O'Keeffe, Acta Crystallogr. B 47 (1991) 192–198.
[17] V. Ting, Y. Liu, L. Norén, R.L. Withers, D.J. Goossens, M. James, C. Ferraris, J. Solid State Chem. 177 (2004) 4428.
[18] R.L. Withers, S. Schmid, J.G. Thompson, Prog. Solid State Chem. 26 (1998) 1–96.
[19] S. van Smaalen, Cryst. Rev. 4 (1995) 79–202.
[20] F.J. Brink, L. Norén, R.L. Withers, J. Solid State Chem. 177 (2004) 2177–2182.